ELSEVIER

Journal of Power Sources 106 (2002) 295–303

JOURNAL OF POWER SOURCES

www.elsevier.com/locate/jpowsour

Performance and lifetime analysis of the kW-class PEMFC stack

S.-Y. Ahn[a], S.-J. Shin[b], H.Y. Ha[b], S.-A. Hong[b], Y.-C. Lee[a], T.W. Lim[c], I.-H. Oh[b,*]

[a]*Department of Chemical Engineering, Sungkyunkwan University, Suwon 440-746, South Korea*
[b]*Fuel Cell Research Center, Korea Institute of Science and Technology, Seoul 136-791, South Korea*
[c]*Fuel Cell Vehicle Team, Hyundai Motor Company, Namyang 445-850, South Korea*

Abstract

A counter-flow type 40-cell proton exchange membrane fuel cell (PEMFC) stack with an effective electrode area of 200 cm^2 has been assembled and its performance was investigated. Under the condition of atmospheric pressure and 75 °C, the maximum power of the stack was 2.89 kW (0.36 W/cm^2 per cell) and 2.3 kW (0.29 W/cm^2 per cell) for H_2/O_2 and H_2/Air, respectively. However, the stack showed a rapid decay in performance after continuous operation of 1800 h. Electron probe micro analyzer (EPMA) and X-ray fluorescence (XRF) spectrometer analyses revealed that degradation of the catalyst and contamination of the polymer electrolyte membrane were the main causes of such sudden decay.

Keywords: Proton exchange membrane fuel cell (PEMFC); Stack; Lifetime analysis

1. Introduction

The proton exchange membrane fuel cell (PEMFC) is an adequate system for the power sources of the zero-emission vehicles, as its current density is higher compared to other types of fuel cells, the stack structure is rather simple, and there is no leakage or loss of electrolyte during the operation. It has also advantages of rapid start-up and response, long endurance, and flexibility of fuel usage from pure hydrogen to methanol and natural gas [1,2]. In addition, because of the various ranges of power, PEMFC can be applied to various fields, such as power sources for stationary generators, space shuttles, road vehicles, and military apparatuses. However, there are various disadvantages to be overcome, too. It cannot utilize waste heat and cannot be directly connected to the fuel processor, because the operating temperature of the PEMFC is too low. The platinum catalyst is too expensive and the CO tolerance limit for platinum is also too low. In addition, the polymer electrolyte membrane is too expensive and it is difficult to control the water content of the polymer electrolyte membrane in operation.

For the PEMFC to be commercialized in mobile and stationary power supplies, a sufficient lifetime of the PEMFC is necessary. For example, at least 5000 and 40,000 h operations are required for fuel cell vehicles and residential power generators, respectively. In practise, the actual lifetime is not sufficient due to the decay in performance. During long-term operation the electrochemical performance may be degraded and the operation behavior may be changed. These effects are induced by a degradation of the fuel cell components, which makes the study of the structural and chemical changes of single components effected by electrochemical stressing necessary for an understanding of the degradation mechanisms and effects [3].

There have been a few reports of the long-term operation of PEMFC stacks. Mitsubishi Electric Corporation has operated 1 kW-class stack for 1200 h under daily start and stop mode [4], and W. L. Gore & Associates Inc. has operated a 10 kW-class stack for 800 h [5]. Ballard Power Systems has successfully operated the Mk6000 short stack for as long as 8000 h [6]. However, few reports have been published to analyze the decay of the stack performance during long-term operation.

In Korea, since the Korea Gas Corporation succeeded in operation of a 1 kW-class PEMFC stack based on E-Tek electrodes in 1996 [7], many organizations have tried to manufacture multi-kW stacks [8–10]. In this study, a 2 kW PEMFC stack made of our own MEAs has been manufactured and not only the initial performance but also its long-term operational behavior were examined. After the long-term operation, the causes of the decay in performance were investigated by various analysis tools.

* Corresponding author. Tel.:+82-2-958-5272; fax:+82-2-958-5199.
E-mail address: oih@kist.re.kr (I.-H. Oh).

0378-7753/02/$ – see front matter
PII: S0378-7753(01)01032-1

2. Experimental

2.1. Stack assembly

The catalytic inks for the electrodes were prepared from Pt/C powders (E-Tek), Nafion solution, and *iso*-propyl alcohol. The inks were then cast by screen printing equipment over the carbon papers to make the electrodes. The Pt loading amounts were 0.4 and 0.7 mg/cm^2 for anode and cathode, respectively. The membrane-electrode assembly (MEA) was prepared by placing the above electrodes at both sides of the pre-treated Nafion 115 membrane, followed by hot pressing at 140 °C and 100 atm for 2 min. The effective electrode area was 200 cm^2.

The PEMFC stack was assembled using the above MEAs and machined graphite bipolar plates. Silicon gaskets prepared by a mold process were placed between bipolar plates to prevent gas leakage and crossover. The flow field gas channel of the bipolar plate was a series-parallel flow pattern. Cooling plates were placed at every other cell to remove heat generated by electrochemical reaction. Bipolar and cooling plates were connected with thermocouples to measure and control the temperature of the stack. The number of cells in the stack was 40 and the specification of the stack is summarized in Table 1.

2.2. Operation and performance evaluation of the stack

At the beginning of the stack operation, the humidified hydrogen and oxygen gases were supplied to both anode and cathode, respectively, by a counter current flow pattern for uniform temperature distribution and gas distribution in the stack. And then the stack was kept moisturized with humidified gases for 24 h at 75 °C. For stack humidification, an external bubbler type humidifier was adopted and the humidities at the anode and cathode inlet were monitored to be almost 100% at the operating temperature. After passing through ultra-filtration and ion exchange membranes, the coolant, which was de-ionized water to prevent short circuits, was supplied to the cooling plates with the same direction as the hydrogen gases, and then recirculated to the water bath. The initial performance and the various properties of the stack were measured when the stack reached the steady state. The stack was operated at a temperature of 75 °C and an operating pressure of 1 atm. The utilization of fuel and oxidant gases were set at $U_f = 0.5$ and $U_o = 0.25$. The performance of the stack was evaluated by measuring the *I–V* characteristics using the electric loader (Daegil Electronics, EL500P).

Table 1
Specification of the stack

Item	Specification
Area of electrode	200 cm^2 (14.1 cm × 14.1 cm)
Number of cells	40
Anode	0.4 mg Pt/cm^2
Cathode	0.7 mg Pt/cm^2
Preparation of electrode	Screen printing method
Electrolyte membrane	Nafion 115
Gas distribution	Counter-flow (internal manifold)
Humidification of gas streams	External bubble humidifier

2.3. Analyses for the causes of the performance degradation of the stack

Various analysis tools have been used to investigate causes of the performance degradation of the stack during the long-term operation. The internal resistance of the each cell in the stack was evaluated under open circuit voltage (OCV) using milliohmmeter (Hewlett Packard, HP4238A). The cell performance degradation by contamination was investigated using SEM (scanning electron microscopy; HITACHI, S-4200, Japan), EPMA (electron probe micro analyzer; JEOL, JXA-8600) and XRF (X-ray fluorescence spectrometer; RIGAKU, RIX-2100). In addition, electrochemical analyses were performed to analyze degradation of the MEA components. The electrochemically active area and the resistance of the MEA were also investigated by a potentiostat/galvanostat (EG&G, M273) and an impedence analyzer (ZAHNER Electrik, IM6), respectively, before and after the continuous operation.

3. Results and discussion

3.1. Performance of the stack

Fig. 1 shows the initial performance of the stack at 75 °C and 1 atm, with a gas utilization of 0.5 for H_2 and 0.25 for O_2. The performance of the stack was measured after it was

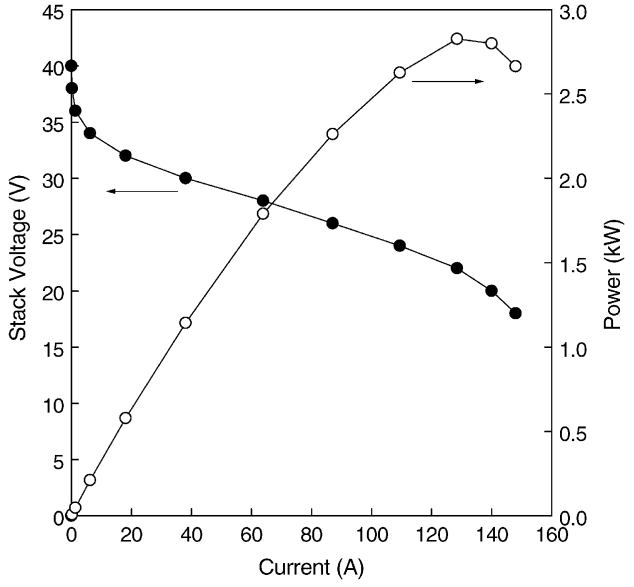

Fig. 1. Initial performance of the stack; $T_c = 75$, $T_f = 75$ and $T_o = 70$ °C; $P = 1$ atm; $U_f = 0.5$ and $U_o = 0.25$.

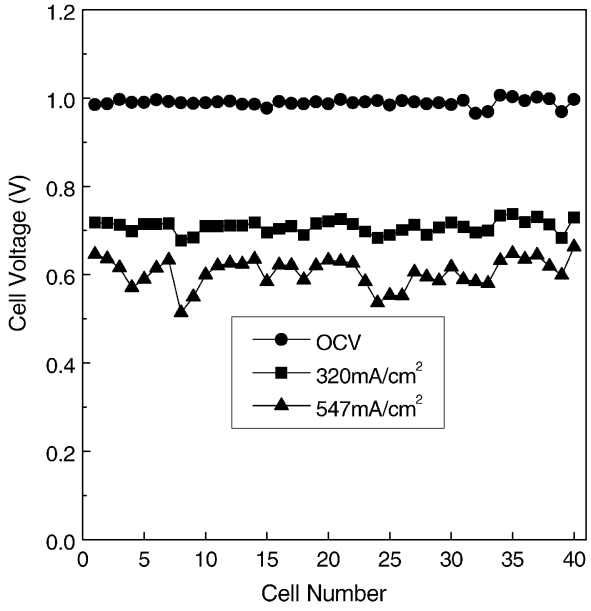

Fig. 2. Distribution of cell voltage in the stack.

kept moisturized with humidified gases for 24 h. As can be seen in the figure, the OCV of the stack was 40.0 V, with the average OCV of each unit cell being 1.00 V. As the load increased to 24 V (0.6 V per cell), the current and power became 109.4 A (547 mA/cm^2) and 2.63 kW (0.33 W/cm^2 per cell), respectively. The maximum current and power, 128.5 A (643 mA/cm^2) and 2.83 kW (0.35 W/cm^2 per cell), could be obtained at 22 V (0.55 V per cell). It can be seen that the OCV value of the stack was lower by 230 mV than that of the theoretical value calculated from the Nernst equation. The discrepancy between the actual and theoretical OCV values, as has been well known, was mainly caused by the mixed potential in the cathode [11].

The voltage distribution of unit cells in the stack is represented in Fig. 2. The nearest cell to the cathode gas inlet was assigned as number 1 cell. The distribution of the OCV for unit cells was uniform but the voltage deviation increased as the load increased. Particularly, the voltages of the 8th, 24–26th cell at the load of 547 mA/cm^2 were lower than other cells. It seems that the electrode polarization for those cells might be influenced by some problems occurred during electrode preparation, stacking, or operation.

Fig. 3 shows the voltage loss analysis of the each unit cell in the stack at a current density of 291 mA/cm^2. The voltage at 291 mA/cm^2 was 28 V (0.7 V per cell) and, therefore, the average voltage loss per unit cell was about 0.3 V per cell. The voltage loss at each unit cell is composed of several factors. The first is the Nernst loss, which is the difference between OCV and the voltage at a current density of zero obtained by extrapolating the *I–V* curve. Although the Nernst loss varies with fuel utilization, the Nernst loss of the stack in this study where pure H_2 and O_2 were used appeared very small. The second one is the voltage loss resulting from the IR drop, which can be measured by

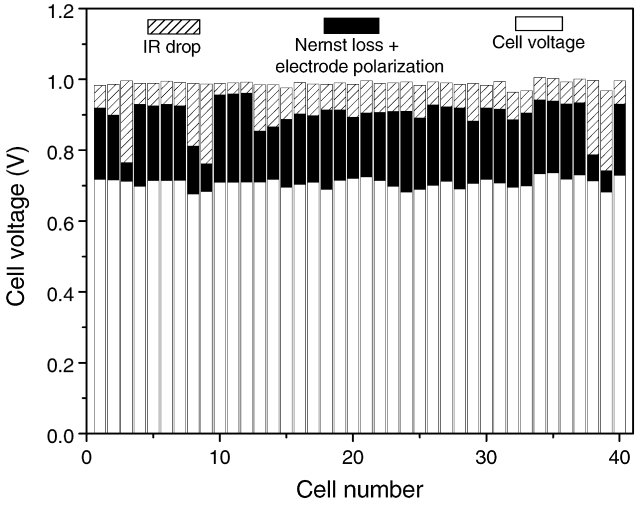

Fig. 3. Voltage loss analysis of the unit cells in the stack.

milliohmmeter. The voltage loss from IR drop was found to be 92 mV per cell at 291 mA/cm^2. Fig. 4 shows the internal resistance of the each unit cell in the stack at 291 mA/cm^2. As can be seen in the figure, the total internal resistance of the stack was 63.1 mΩ and the average of the individual cells was 1.58 mΩ. It is seen from Figs. 3 and 4 that the voltage loss caused by the internal resistances of the 3rd, 8th, 9th, 38th and 39th cells was higher than the those of other cells. The last factor is the electrode polarization, which can be estimated from the relationship that the sum of the Nernst loss, the IR drop loss, and the electrode polarization equals the actual voltage loss. If we assume that the Nernst loss is negligible, then the electrode polarization becomes 208 mV per cell, which is almost double compared to the IR drop loss. Therefore, reduction of the electrode polarization by the improvement of the electrode preparation process is an effective way to increase the cell performance.

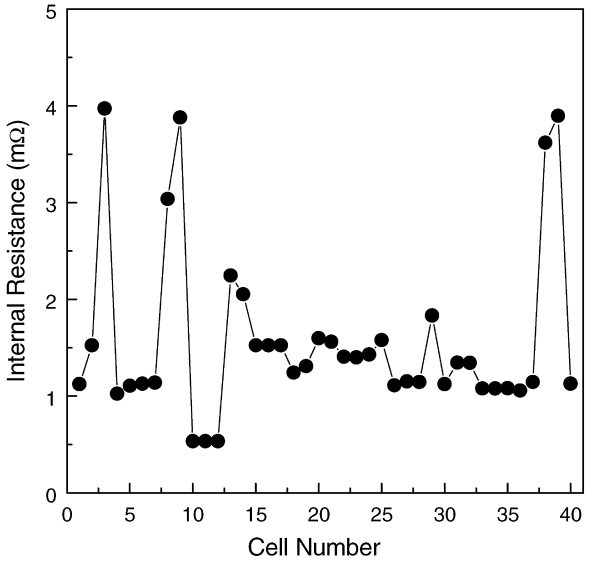

Fig. 4. Distribution of internal resistance in the stack at OCV condition.

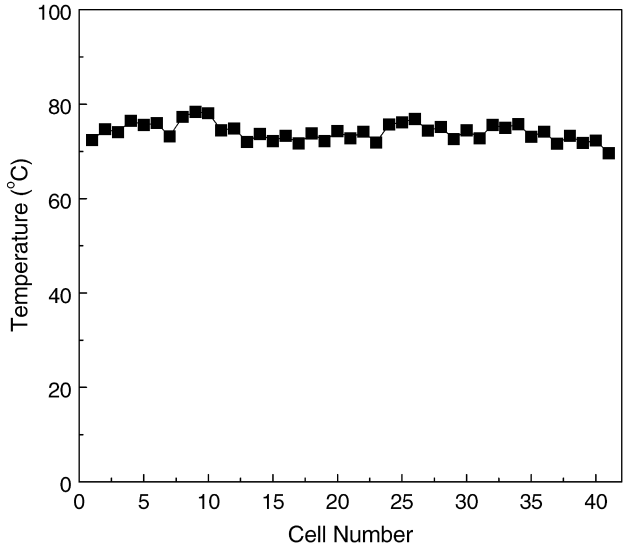

Fig. 5. Distribution of cell temperature in the stack at 70 A (350 mA/cm^2) and 25.7 V (0.64 V per cell).

Fig. 5 shows the temperature distribution of unit cells in the stack where the cooling plates were placed at every other cell to remove heats generated by electrochemical reaction. The temperature distribution was measured at 70 A with controlling the stack temperature at 75 °C. As can be seen in the figure, the temperature distribution was almost uniform on the whole, with a deviation of ±5 °C. It is important that generated heat is effectively removed during stack operation. Any cell showing a severe deviation may result in a performance degradation. For example, flooding of the cell caused by lower temperature may increase the mass transfer resistance and drying of the cell caused by higher temperature may reduce the proton-conducting rate of the polymer electrolyte membrane. In this study, however, no such effect from the temperature deviation occurred.

Oxygen gain is the amount of voltage drop of the cell when the cathode gas is changed from pure oxygen to air with the same oxygen molarity and it is regarded as an index of the mass transfer resistance of oxygen in the cathode. Fig. 6 shows the effect of oxidants on the *I–V* characteristics and the power of the stack when the utilizations of oxidant and fuel were 0.25 and 0.5. At the stack voltage of 24 V (0.6 V per cell), the stack currents for oxygen and air were 112 A and 88.4 A, respectively. Therefore, it was seen that the performance of the stack decreased 21.1% when oxidant was changed from oxygen to air. The oxygen gain increases with an increase in load in general, because the slopes of *I–V* curves in Fig. 6 are not the same. It can be deduced from this result that a pressurized operation will be required to increase the stack performance.

3.2. Continuous operation and lifetime analyses of the stack

Fig. 7 shows the result of 1800 h continuous operation of the stack when it was operated at a gas utilization of 0.5 for H_2 and 0.25 for air. Although non-uniform distribution in voltage of the unit cells in the stack was observed, continuous operation of the stack up to 1800 h was possible; namely, for 300 h under full load and for 1500 h under partial load. The continuous operation of the stack was composed of three parts. The first period from (I) to (III) was a warming-up step of the stack and the system for continuous operation under partial load. The second period from (IV) to (V) was the operation at 70 A under full load. At that time, the power of the stack was about 1.75 kW. The

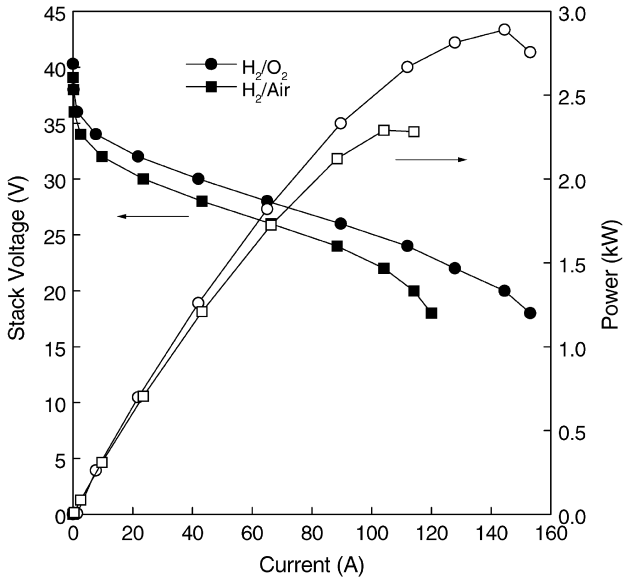

Fig. 6. Effect of oxidants on the stack performance.

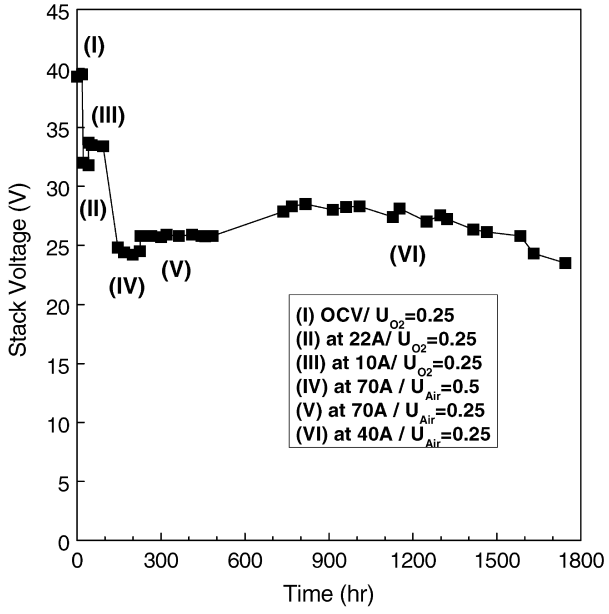

Fig. 7. Performance of the stack during the continuous operation; $T_c = 75$, $T_f = 75$ and $T_o = 70$ °C; $P = 1$ atm; and $U_f = 0.5$.

third period (VI) was the operation at 40 A under partial load. During the third period, the stack was operated under partial load of 40 A for 12 h in a day, and for the other half day, it was operated at OCV. As can be seen in the figure, the performance of the stack did not decrease during the second period from (IV) to (V), but it reduced slowly with an average decay rate of 4.37 mV/h during the third period (VI), and then after continuous operation of 1800 h, the stack showed the rapid decay in performance. It was thought that careless operation of the stack might cause the rapid decay of the stack performance, because the stack was exposed to flooding at that time. There may be several factors affecting the performance drop of the stack after the continuous operation, and these have been investigated with the various analyzing tools as follows.

After continuous operation of 1800 h, the components of the MEA have been analyzed to investigate the reason for the rapid decay in performance of the stack. When the stack was disassembled, it was observed that the silicon gasket was attached firmly to the Nafion electrolyte membrane. Fig. 8 shows the SEM images of the pure Nafion and the one after the disassembly. As can be seen in the SEM images, the silicon gasket was buried beneath the Nafion membrane surface. It is believed that some of the silicon gasket dissolved and then penetrated the Nafion membrane due to the acidity of the moisturized Nafion which corresponds to 1 M sulfuric acid solution.

Gulzow et al. [3] have reported that during operation, dispersion of the platinum catalyst of both electrodes was changed due to the electrochemical stress during the stack operation. Namely, on the anode side, platinum–hydrogen complexes were formed and then migrated from the anode to the interface between anode and the Nafion membrane, and on the cathode side, platinum oxides were formed and then migrated from the cathode to the backing of the cathode. If silicon is dissolved in the membranes, then it will also migrate from the anode to the cathode side due to the electrochemical stress. The silicon gasket originally contacts only the Nafion membrane without the direct contact with the electrode in the MEA and, thus, there should not be any Si in the membrane, nor in the electrode.

Therefore, the edge of the MEA near the silicon gasket was analyzed by the EPMA line profile technique to check the contamination and degradation of the MEA. The physical characterization of new and electrochemically stressed MEA is a suitable tool to investigate the contamination and degradation of the MEA components. Fig. 9 shows results of the EPMA analysis for the dispersion of Pt, Si, and O in the MEA. As can be seen in the EPMA images, Pt peaks existed in the catalytic layers of anode and cathode in all cases. In

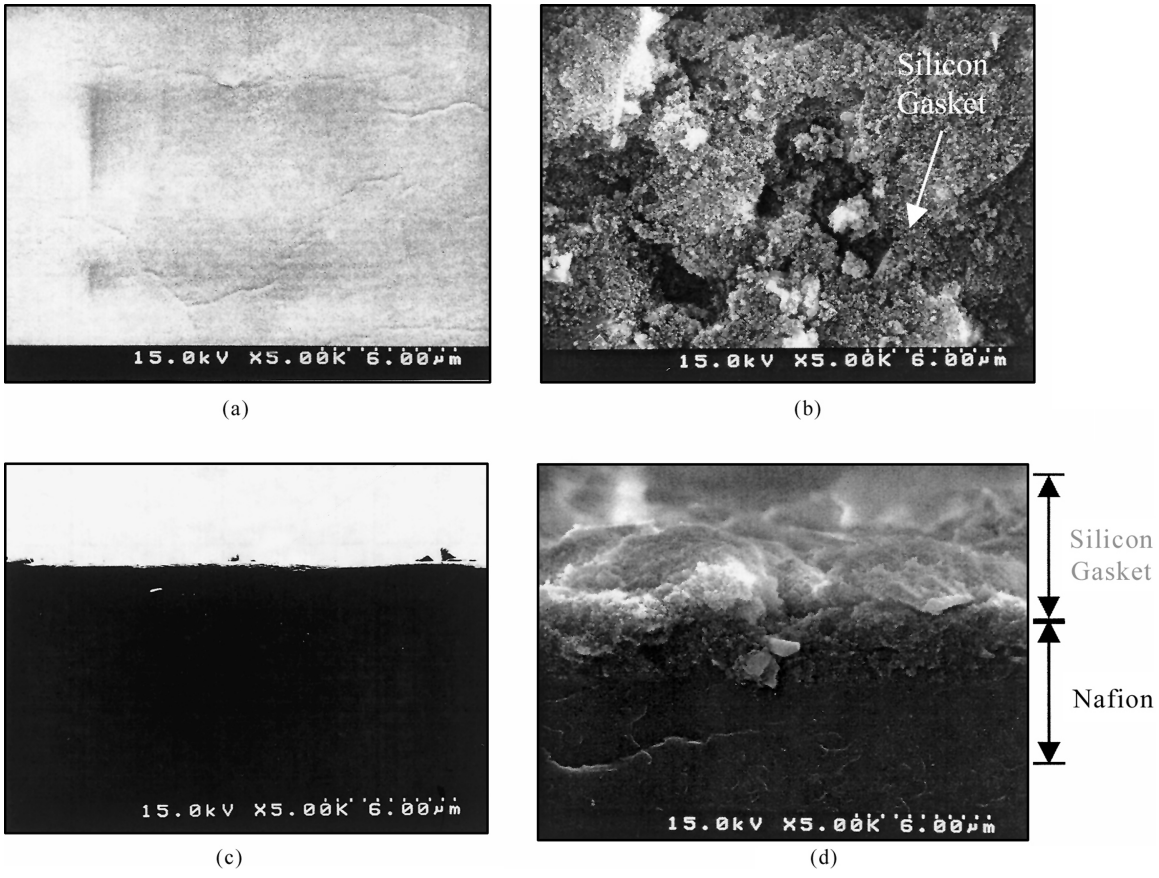

Fig. 8. SEM images of the Nafion 115 before and after 1800 h operation. (a) Surface, before; (b) surface, after; (c) cross-section, before; (d) cross-section, after.

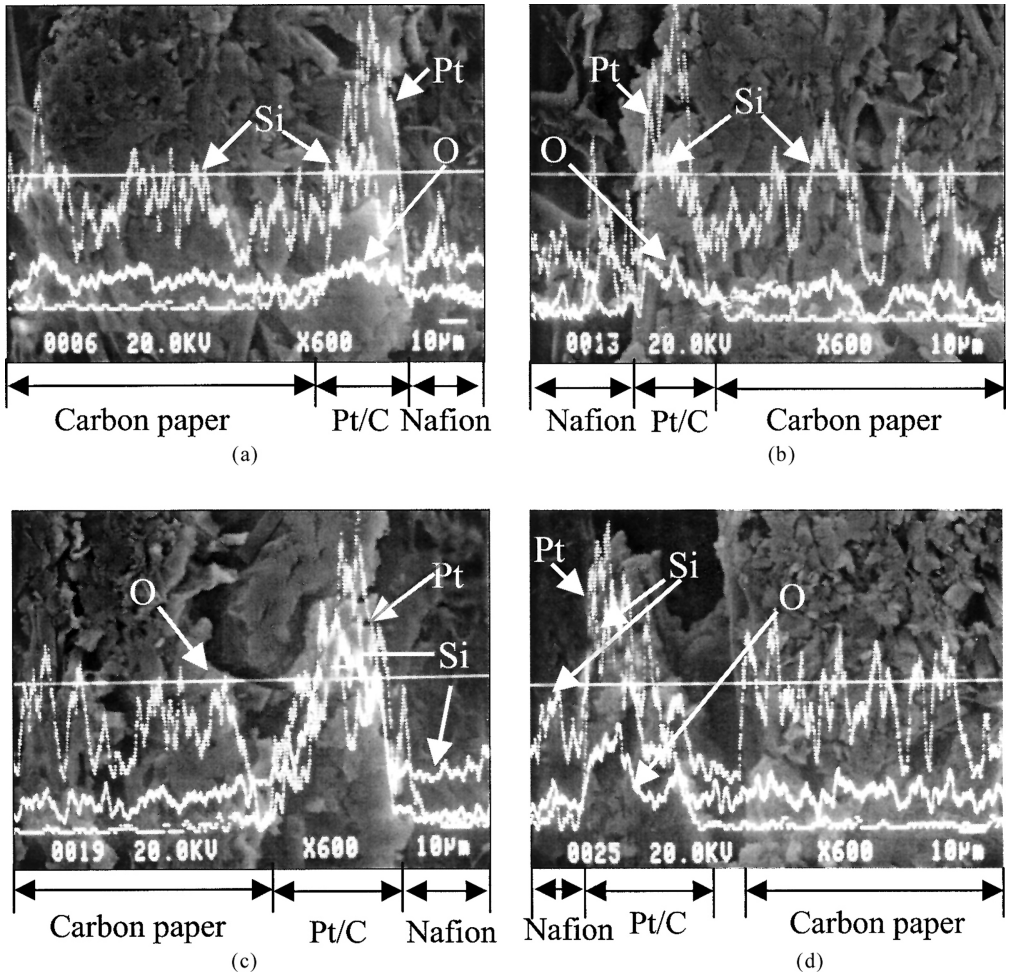

Fig. 9. EPMA images of the MEA before and after 1800 h operation. (a) Anode, before; (b) cathode, before; (c) anode, after; (d) cathode, after.

case of Si, however, Si peaks did not appear in the pure MEA before operation; whereas they existed in the electrochemically stressed MEA after operation. Particularly, Si was detected in the catalytic layers of the anode and the cathode and also at the surface of the Nafion membrane near the catalytic layer. In the case of oxygen, O peaks also appeared after the operation and they existed at the catalytic layer of the electrochemically stressed cathode as a form of platinum oxide. However, we could not confirm the existence of the platinum–hydrogen complexes because no Pt peaks of the electrochemically stressed anode appeared between the catalytic layer and the Nafion membrane.

It is seen from the Pt and O peak distribution that platinum oxide was formed at the catalytic layer of the electrochemically stressed cathode, although it did not migrate to the backside of the cathode as indicated by Gulzow et al. [3]. The existence of platinum oxide in the catalytic layer of the cathode strongly suggests that the catalysts in the cathode were degraded. The Si peak distribution implies that Si was dissolved into the Nafion membrane first and then migrated through the membrane, followed by penetration into the catalytic layer of the electrochemically stressed MEA. It may be concluded from these analyses that the catalysts in the cathode were degraded by the formation of platinum oxide and the catalysts and Nafion membrane were contaminated by silicon which was dissolved from the gasket.

The possibility that the Nafion membrane and the MEA exposed to the coolant was contaminated by impurities in the coolant was examined by the XRF technique. The amounts of impurities in the coolant are shown in Table 2, and those in the MEA along a section are summarized in Table 3. It is seen from the table that Si, Al, S, K, Fe and Cu existed in the

Table 2
The results of XRF analysis for impurities in the coolant after continuous operation

Elements	Amounts (wt.%)
Al	10^{0}
Si	$10^{0\sim1}$
S	10^{-1}
K	10^{-2}
Fe	10^{-2}
Cu	10^{-2}
Cl	10^{-2}
V	10^{-3}
Cr	10^{-3}

Table 3
The results of XRF analysis for the impurities in the MEA along the position after continuous operation (unit: wt.%)

Distance from edge of the MEA	Elements									
	Al	Si	S	K	Fe	Cu	Ni	Zn	Pb	Pt
0	10^{-2}	10^{0}	10^{0}	10^{-2}	10^{-2}	10^{0}	10^{-2}	10^{0}	10^{-2}	$10^{0\sim1}$
1/3	10^{-2}	$10^{-1\sim0}$	10^{0}	10^{-2}	10^{-2}	10^{0}	10^{-2}	10^{0}	10^{-2}	$10^{0\sim1}$
2/3	–	$10^{-1\sim0}$	10^{0}	10^{-2}	10^{-2}	10^{0}	10^{-2}	$10^{-1\sim0}$	10^{-3}	$10^{0\sim1}$
3/3 (center of the MEA)	10^{-2}	$10^{-1\sim0}$	10^{0}	10^{-2}	10^{-2}	$10^{-1\sim0}$	10^{-2}	$10^{-1\sim0}$	10^{-3}	$10^{0\sim1}$

coolant and they were also detected at most regions of the MEA. It is confirmed from the analyses that contaminants from the coolant contaminated the MEA through the Nafion membrane and the existence of such impurities might inhibit the proton conduction.

Fig. 10 shows the images of the MEA before and after the operation using the EPMA back scattered image (BSI) technique to examine the contact between the electrodes and the Nafion membrane. As can be seen in the figures, the catalytic layer of the electrochemically stressed cathode was separated from the carbon paper. This was because the cathode side was affected by the mechanical stress due to water generated by the electrochemical reaction. This result is consistent with the results of the internal resistance measurement using milliohmmeter. For example, the internal resistance of the 34th unit cell in the stack was 1.1 mΩ before operation, however, it increased to 13.6 mΩ after operation.

Additional electrochemical analyses were carried out. Fig. 11 shows the results of cyclic voltammetry to compare the electrochemical reaction area before and after operation. If the hydrogen oxidation and hydrogen desorption peak areas before and after operation are compared, then it is seen that the hydrogen oxidation and hydrogen desorption peak areas decreased after operation. For example, the hydrogen oxidation peak area decreased about 23% after continuous

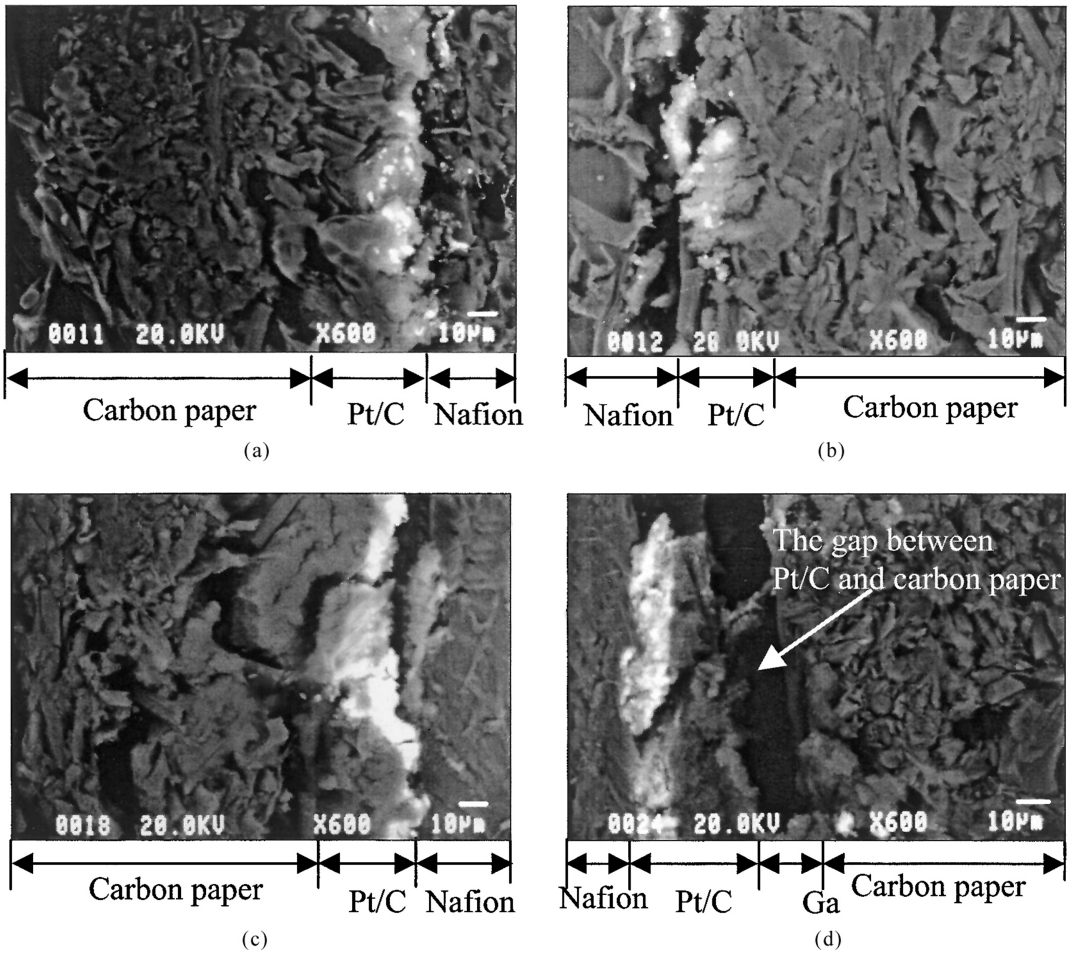

Fig. 10. BS images of the EPMA for MEA before and after 1800 h operation. (a) Anode, before; (b) cathode, before; (c) anode, after; (d) cathode, after.

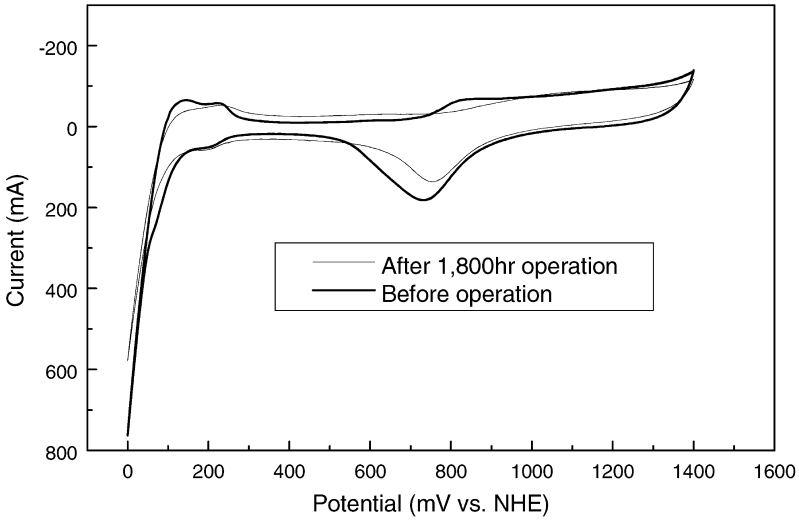

Fig. 11. Cyclic voltammograms before and after 1800 h operation. Scan rate = 50 mV/s, Ca./An. = 0.4/0.7 mg Pt/cm^2, Ca./An. = N_2/H_2, $T = 75$ °C and $P = 1$ atm.

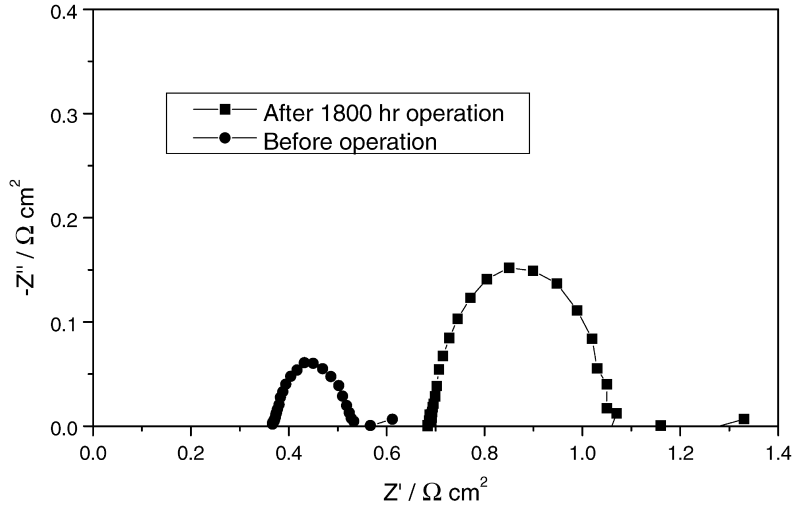

Fig. 12. Nyquist plots before and after 1800 h operation. Ca./An. = 0.4/0.7 mg Pt/cm^2, Ca./An. = O_2/H_2, $V = 0.8$ V, $T = 75$ °C and $P = 1$ atm.

operation. Fig. 12 shows the results of AC impedance analysis at 0.8 V to compare polarization resistance before and after operation. As can be seen in the figure, after continuos operation of the stack, the electrolyte resistance and the charge transfer resistance were increased 1.8 and 5.8 times, respectively. Therefore, it implies that the interface of the electrode and the Nafion membrane was separated and contaminated gradually as the operation time elapsed.

4. Conclusions

A counter-flow type 40-cell PEMFC stack with an effective electrode area of 200 cm^2 has been assembled and its performances and lifetime were investigated. Under conditions of atmospheric pressure and 75 °C, the maximum power of the stack was 2.89 kW (0.36 W/cm^2 per cell) and 2.3 kW (0.29 W/cm^2 per cell) for H_2/O_2 and H_2/Air, respectively. The analysis of the factors causing voltage losses revealed that polarization resistance of the electrodes was the main reason. Although non-uniform distribution in voltage of the unit cells in the stack was observed, continuous operation of the stack up to 1800 h was possible; namely, for 300 h under full load and for 1500 h under partial load. However, after continuous operation for 1800 h, the stack showed a rapid decay in performance. The reasons for such sudden decay were investigated by employing various analytical techniques. EPMA analysis of the MEA shows that a significant amount of silicon were detected at the catalytic layer of both anode and cathode, and oxygen existed at the cathode as a platinum oxide. XRF analysis of the coolant also confirmed the existence of various inorganic materials. As a result of the analysis, it was concluded that degradation of the catalyst and contamination

of the MEA might have led to the failure of the long-term stack performance.

References

[1] L.J.M.J. Blomen, M.N. Mugerwa, Fuel Cell System, Plenum Press, New York, 1993.
[2] K. Kordesch, G. Simander, Fuel Cell and Their Applications, VCH, Weinheim, Germany, 1996.
[3] E. Gulzow, H. Sander, N. Wagner, M. Lorenz, A. Schneider, M. Schulze, Fuel Cell Seminar Abstracts, Portland, 2000, p. 156.
[4] H. Maeda, H. Fukumoto, K. Mitsuda, H. Urushibata, M. Enami, K. Takasu, Fuel Cell Seminar Abstracts, Orlando, 1996, p. 272.
[5] F. Barbir, F. Marken, B. Bahar, J.A. Kolde, Fuel Cell Seminar Abstracts, Orlando, 1996, p. 505.
[6] K. Washington, Fuel Cell Seminar Abstracts, Portland, 2000, p. 468.
[7] Y.-T. Ko, Development of the 1 kW-Class PEMFC Stack, Department of Trade and Industry, 1996.
[8] H.-J. Choi, S.-Y. Ahn, S.-A. Cho, J.-K. Lee, J.-P. Shim, S.-Y. Cha, H.Y. Ha, S.-A. Hong, T.W. Lim, I.-H. Oh, Hwahak Konghak 38 (4) (2000) 550.
[9] S.-Y. Ahn, I.-H. Oh, H.Y. Ha, H.-J. Choi, S.-A. Cho, S.-A. Hong, T.-W. Lim, Theor. Appl. Chem. Eng. 5 (2) (1999) 3393.
[10] Y.-G. Chun, D.-H. Peck, T.-H. Yang, C.-S. Kim, D.R. Shin, Theor. Appl. Chem. Eng. 5 (2) (1999) 3389.
[11] J. O'M Bockris, S. Srinivasan, Fuel Cells: Their Electrochemistry, McGraw-Hill, New York, 1969.